



1 **Fossil-Dominated SOA Formation in Coastal China: Size-Divergent**
2 **Pathways of Aqueous Fenton Reactions versus Gas-phase VOC**
3 **Autoxidation**

4 Jia-Yuan Wang, Meng-Xue Tang, Shan Lu, Ke-Jin Tang, Xing Peng, Ling-Yan He, Xiao-Feng
5 Huang

6 Key Laboratory for Urban Habitat Environmental Science and Technology, School of Environment and
7 Energy, Peking University Shenzhen Graduate School, Shenzhen, 518055, China.

8 Corresponding author: Meng-Xue Tang (tangmx@pku.edu.cn)

9

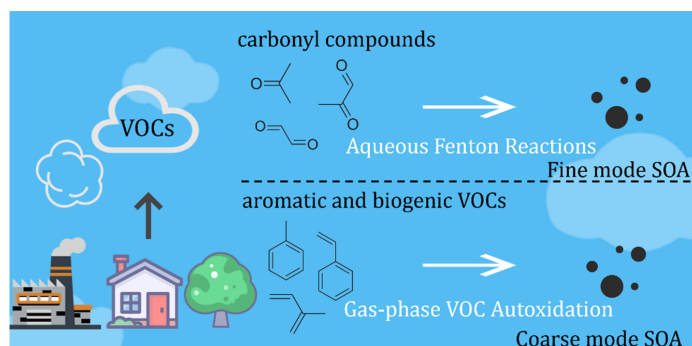


10 **Abstract:** Elucidating size-dependent formation mechanisms of secondary organic aerosols (SOA)
11 remains a critical research gap in atmospheric chemistry. Here, we analyzed water-soluble compounds
12 in size-segregated aerosol samples (0.056–18 μm) collected at a coastal site in southern China.
13 Radiocarbon (^{14}C) isotope analysis reveals that fossil sources dominate SOA in both fine (95.8%) and
14 coarse (80.4%) modes, while the small amount of biogenic SOA mostly existed in the coarse mode
15 (74.1%). Fine-mode oxygenated organic carbon (OOC) correlates strongly with polar carbonyl
16 compounds (e.g., glyoxal, methylglyoxal, acetone, and MVK+MACR), while coarse-mode OOC
17 exhibits better correlations with nonpolar aromatic hydrocarbons (e.g., toluene, C8 aromatic, C9 aromatic,
18 styrene) and biogenic VOCs (e.g., monoterpenes, isoprene), indicating that the sources of fine- and
19 coarse-mode OOC are different. Multivariate analyses incorporating inorganic ions, pH, water-soluble
20 iron ions, aerosol liquid water content, and O_3 revealed divergent size-dependent mechanisms,
21 emphasizing the significant role of aqueous-phase reactions in fine-mode OOC formation, particularly
22 the key contribution of water-soluble Fe ions ($r^2 = 0.74$), while coarse-mode OOC exhibited a notable
23 correlation with O_3 ($r^2 = 0.63$). Combining the information on VOCs precursors and key components,
24 our study elucidates that aqueous-phase reactions play a key role in fine-mode OOC, especially the
25 Fenton reaction, while gas-phase VOC autoxidation plays an important role in the coarse-mode OOC
26 generation. By examining OOC formation across a wide range of particle sizes, our study highlights the
27 critical need for mode-specific treatment of SOA generation in atmospheric chemical transport modeling.

28 **Key words:** Secondary organic aerosol (SOA), Fine mode, Coarse mode, Aqueous-phase reactions, Gas-
29 phase autoxidation
30



31 **Graphical abstract:**



32



33 1.Introduction

34 In urban areas, organic aerosol (OA) constitutes 30-70% of submicron particle mass(Zhang et al.,
35 2017b) and has significant impacts on human health, radiation balance, and air quality. OA can originate
36 from direct emissions, known as primary organic aerosol (POA), or be formed in the atmosphere through
37 the oxidation of semi-volatile and volatile organic compounds (VOCs) followed by nucleation or
38 condensation of oxidation products onto the preexisting particles., resulting in secondary organic aerosol
39 (SOA) (Peng et al., 2021). Globally, SOA is estimated to contribute up to 93% of the total OA budget
40 (Hallquist et al., 2009). However, our understanding of the SOA formation mechanisms is still limited,
41 the complexities of SOA formation are not only due to the presence of large amounts of biogenic and
42 anthropogenic VOC precursors, but also because each VOC can undergo a number of atmospheric
43 degradation processes (e.g., gas-phase radical-mediated oxidation, heterogeneous oxidation, and
44 oligomerization) to produce various condensable oxidized organics (COO) with distinct functionality,
45 reactivity, and volatility(Gu et al., 2023; Xu et al., 2017; Yu et al., 2016).

46 Secondary organic aerosol (SOA) can be formed from the atmospheric oxidation of volatile organic
47 compounds (VOCs) or originate from various processes such as heterogeneous reactions, photochemistry,
48 and aqueous-phase oxidation (Dominutti et al., 2022). Field studies on SOA formation mostly focused
49 on fine particles (PM₁) partly because of instrument limitations (Xu et al., 2017; Yao et al., 2022a), recent
50 mass spectrometry-based studies have shown that photochemical oxidation has been suggested to be the
51 major pathway of SOA formation, photochemical oxidation of VOCs is generally initiated by reactions
52 with radicals (e.g., OH, NO₃) or oxidants (e.g., O₃), producing a variety of condensable oxidized organics
53 (COO) types, which subsequently engage in gas-to-particle conversion to contribute to SOA
54 formation(Xu et al., 2017; Zhan et al., 2021).However, aqueous-phase formation of SOA has also been



55 considered an important pathway, SOA can form in the aqueous phase on wet aerosols, clouds, and fogs
56 through further chemical processes involving water-soluble organic compounds or the organic products
57 of gas-phase photochemistry (Ervens et al., 2011; Gu et al., 2023; Mei et al., 2025).

58 While that formed on coarse particles was mostly neglected, dust (both natural and
59 anthropogenically emitted dust) is constantly present in the atmosphere and is one of the largest
60 contributors to aerosol mass in the troposphere (Wu et al., 2024; Xu et al., 2024), exerting a significant
61 impact on global climate by modulating radiative balance. Dust particles mainly consist of
62 aluminosilicate, sea salt, SiO_2 , CaCO_3 , and coated with secondary organic and inorganic aerosol
63 components under an ambient environment (Li & Shao, 2009; Yang et al., 2024), dust particles act as
64 reactants or catalysts, enhancing atmospheric heterogeneous reactions and photochemical processes (Pan
65 et al., 2023; Wang et al., 2020b). Heterogeneous reactions and photochemical reactions on mineral dust
66 may play an important role in coarse modal SOA generation (George et al., 2015; He et al., 2022a; Wang
67 et al., 2020b). This also suggests that different formation mechanisms may govern fine-mode and coarse-
68 mode secondary organic aerosols.

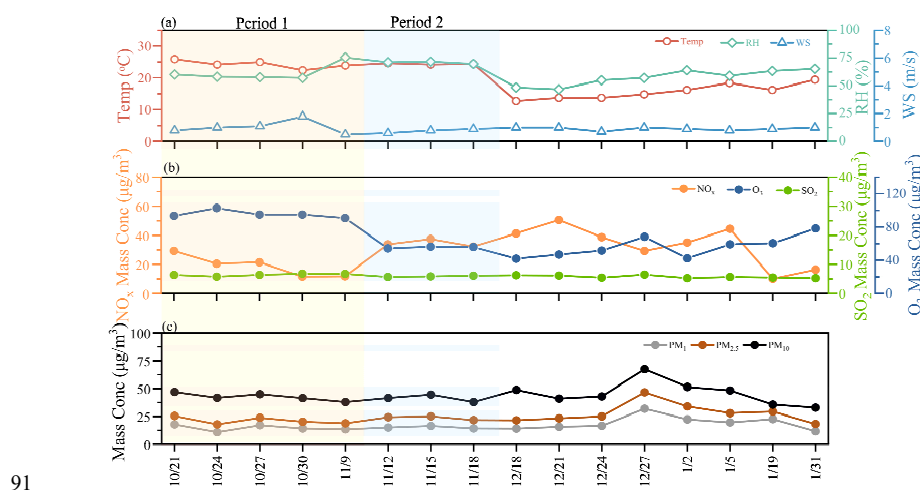
69 In this study, we collected a broad range of size-segregated samples (0.056–18 μm) from Shenzhen,
70 a coastal city in southern China, to obtain comprehensive particle size information. We utilized the offline
71 ACSM-PMF method to characterize SOA in these samples and combined it with ^{14}C analysis to gain a
72 deeper understanding of SOA from fossil fuel and biogenic sources (He et al., 2022a; Huang et al., 2020).
73 This study explores the mechanisms of SOA formation across both fine-mode and coarse-mode,
74 enhancing our understanding of the diverse generation mechanisms of SOA across various particle size
75 distributions.



76 2. Material and methods

77 2.1 Sampling site and sample collection

78 The sampling site, Atmospheric Observation Supersite of Shenzhen (AOSS, 22.60 °N, 113.98 °E), is
79 located at an urban site in the southeast of the PRD region. There are no significant local pollution sources
80 in the vicinity. The sampling period encompassed both the peak of particulate matter pollution and the
81 most severe photochemical pollution in Shenzhen for the year. Atmospheric volatile organic compounds
82 (VOCs) levels at this site are typically influenced by continental air masses, marine air masses, and local
83 biogenic emissions (Li et al., 2024a). A ten-stage micro-orifice uniform deposit impactor (MOUDI, model
84 110, MSP Co., USA) with aerodynamic diameter cut-points of 0.056, 0.1, 0.18, 0.32, 0.56, 1.0, 1.8, 3.2,
85 5.6, 10, and 18 μm was used to collect size-segregated aerosol samples on Teflon filters from 21 October
86 2022 to 3 February 2023. In this study, we found that 1-1.8 μm particles showed more coarse mode
87 properties, so we took 1 μm as the division boundary, so we use 1 μm as the boundary between
88 fine particles and coarse particles, in this study. The sampling flow rate was 30 L/min. The average
89 ambient temperature during the sampling period was 20.0 °C, and the dominant wind direction was
90 northeasterly. In total, one hundred and sixty samples were collected with a sampling cycle of 72 hours.



92 **Figure 1.** Time series of relative humidity (RH), Temperature (Temp) and wind speed (WS) (a), O_3 ,
93 SO_2 and NO_x (b), PM_{10} , $\text{PM}_{2.5}$ and PM_1 (c). The time series were categorized to be two typical periods
94 based on total O_3 mass concentrations: the high- O_3 period (Period 1), and the low- O_3 period (Period 2)



95 **2.2. Chemical analysis**

96 The mass of the size-segregated aerosol samples was obtained from the difference in mass of the
97 Teflon filter before and after sampling in a cleanroom at conditions of 22.1 °C and 49.2% relative
98 humidity. Then, each filter was extracted with 20 mL of ultrapure water in an ultrasonic bath with ice for
99 30 min and then filtered with a 0.22 µm Teflon filter for further analysis. A portion of the water extract
100 was analyzed for water-soluble metal elements using an inductively coupled plasma mass spectrometer
101 (ICP-MS, Bruker auroraM90, Germany). Inorganic ions (Cl^- , SO_4^{2-} , NO_3^- , NH_4^+ , Na^+ , K^+ , Mg^{2+} , Ca^{2+})
102 were measured using an ion chromatography system (ICS-6000, Dionex, USA). A portion was analyzed
103 for water-soluble organic matter (WSOM) and the corresponding mass spectra using a Nebulizer-ACSM
104 system (ToF-ACSM-X, Aerodyne Research, Inc., USA) and a portion was analyzed for water-soluble
105 organic carbon (WSOC) with a total organic carbon analyzer (N/C 3100, Analytik Jena AG, Germany)
106 to quantify organic oxygen (WSOO, WSOM), the major ion fragments (m/z 44, m/z 57, m/z 65, m/z 93)
107 and elements (C, H, O, and N) measured by ToF-ACSM-X. Equal amounts of the water extract from the
108 same MOUDI stages were combined and concentrated for ^{14}C analysis based on accelerator mass
109 spectrometry. More details of the Nebulizer-ACSM and radiocarbon can be found in (He et al., 2022a;
110 Huang et al., 2020).

111 **2.3 Other measurements**

112 A meteorological monitoring instrument (WXT536, Vaisala, Finland) was used to measure the
113 meteorological variables, including atmospheric temperature (Temp), relative humidity (RH), wind
114 direction (WD), and wind speed (WS). Criteria air pollutants were monitored using the following
115 instruments: a 5030i $\text{PM}_{2.5}$ and 5030i PM_{10} for particulate matter, a 43i SO_2 analyzer, a 42i NO_x analyzer,
116 a 49i O_3 analyzer, and a 48i CO analyzer (Thermo Scientific, USA). Additionally, PTR-ToF-MS (6000X2,



117 Ionicon Analytik GmbH, Austria) with H_3O^+ ionization mode was used for online measurements of
118 volatile organic compounds at the same site during the campaign. Further details regarding the PTR-ToF-
119 MS are available in (He et al., 2022b; Li et al., 2024b).

120 **2.4 Data analysis**

121 The inorganic ion components of size-segregated aerosol samples (Cl^- , SO_4^{2-} , NO_3^- , Na^+ , NH_4^+ , K^+ , Mg^{2+} ,
122 Ca^{2+}), along with relative humidity (RH) and temperature were input into ISORROPIA II model to
123 calculate the aerosol liquid water content (ALWC) and aerosol pH ($\text{pH}_{\text{aerosol}}$), the thermodynamic
124 equilibrium model ISORROPIA II was used to estimate the size-resolved ALWC and $\text{pH}_{\text{aerosol}}$ in this
125 study owing to its accuracy, reliability, and high computational efficiency (Duan et al., 2020; Tan et al.,
126 2017; Xu et al., 2024). The Pearson correlation method was applied using SPSS Statistics software for
127 correlation analysis. Quantitative source apportionment of water-soluble organic carbon (WSOC) was
128 conducted with the U.S. EPA PMF v5.0 software. Data matrices and error matrix of WSOC, WSOO,
129 CO_2^+ , C_4H_9^+ , and nss-K^+ for a total of 160 samples (16 sets \times 10 stages) were input into the PMF model,
130 the three-factor (the more oxidized oxygenated organic carbon (MO-OOC), the less oxidized OOC (LO-
131 OOC), and biomass-burning organic carbon (BBOC) determined to be the most reasonable solution
132 (Figure S1). More details of the source apportionment of WSOC by PMF modeling are provided in the
133 supporting information.

134 **3 Results and discussion**

135 **3.1 average size distributions of the aerosol components**

136 Figure 2a shows the average size distributions of the aerosol components, coarse modes exhibit higher
137 mass concentrations, accounting for 66.7% of the total mass. These coarse modes contain more water-



insoluble components, it contains a variety of metal oxides (i.e., TiO_2 and Fe_2O_3) (Adebiyi et al., 2023). Unlike the coarse mode, the fine mode has a higher proportion of water-soluble components. As is shown in Figure 2b, the main water-soluble inorganic ions in the fine mode differ from those in the coarse mode, sulfate (SO_4^{2-}) and ammonium (NH_4^+) are the most abundant compounds in the fine mode, constituting 17.0% and 7.4% of the total mass of fine particles, respectively. In contrast, nitrate (NO_3^-) and calcium (Ca^{2+}) are the predominant inorganic ions in the coarse mode, comprising 5.6% and 1.5% of the total mass of coarse particles, respectively. Although the compositions of fine- and coarse-mode water-soluble inorganic ions differ significantly, water-soluble organic matter (WSOM) is the most abundant water-soluble component in both modes. WSOM constitutes 55.9% of the total water-soluble mass in fine particles and 40.9% in coarse particles, underscoring its critical role in both size modes.

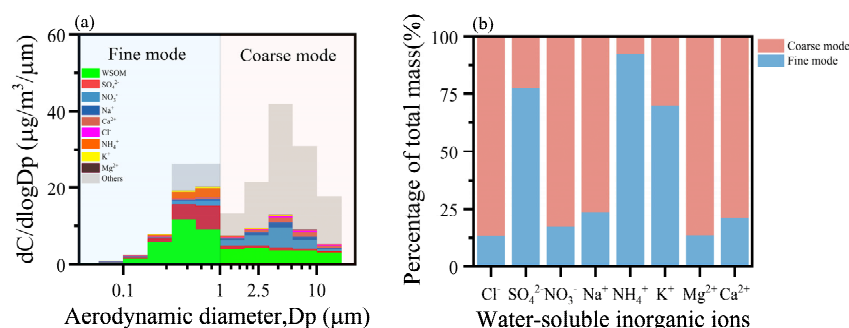


Figure 2. The average size distributions of aerosol components at this site (a), the percentage of the fine mode and coarse mode of water-soluble inorganic ions (b).

3.2 Possible sources of fine and coarse mode SOA

In this study, PMF is used to extract OA components. Figure 3a shows the contributions of the Oxygenated organic carbon (OOC; sum of MO-OOC and LO-OOC) and BBOC in all size bins. The results indicate that BBOC was mainly disturbed in the fine mode accounting for 91.1% of the total



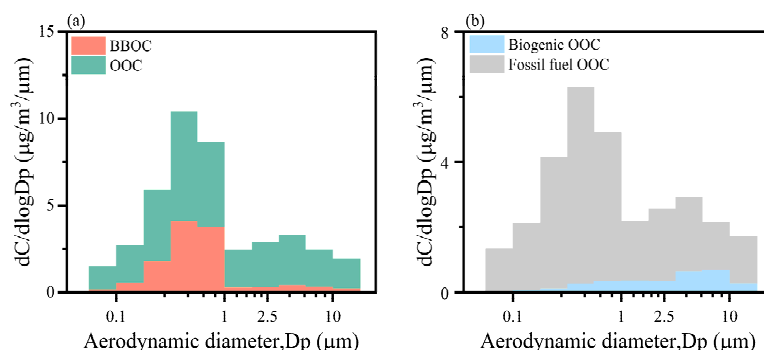
155 BBOC. OOC dominated in both the fine (64.4%) and coarse mode (88.4%), and previous studies found
156 that the fine mode SOA can be estimated by WSOC after removing the contribution of biomass
157 burning(He et al., 2022b; Huang et al., 2020), in this study , OOC is equivalent to SOA. This highlights
158 the critical role of SOA in both the fine and coarse mode.

159 Figure 3b shows the size distributions of fossil fuel OOC and biogenic OOC in all size bins, which were
160 calculated by combining the results from the PMF factor contributions and the ^{14}C isotope analysis, and
161 the calculations were performed as in our previous study with equations (1)-(3) (He et al., 2022a;
162 Huang et al., 2020) :

$$163 \quad \text{biogenic carbon} = \text{WSOC} * f_{\text{modern}} \quad (1)$$

$$164 \quad \text{biogenic OOC} = \text{biogenic carbon} - \text{BBOC} \quad (2)$$

$$165 \quad \text{fossil fuel OOC} = \text{LO-OOC} + \text{MO-OOC} - \text{biogenic OOC} \quad (3)$$



166
167 **Figure 3.** Average size distributions of the WSOC compositions, OOC and BBOC (a), fossil fuel OOC
168 and biogenic OOC(b).

169 After removing the contributions from BBOC, the results clearly indicate that fossil fuel organic
170 carbon (OOC) dominates in both fine (95.8%) and coarse (80.4%) modes, reflecting the significant role



of anthropogenic sources in SOA generation. Regarding particle size distribution, fossil fuel OOC is predominantly found in the fine mode (66.0%), while biogenic OOC is mainly present in the coarse mode (74.1%). This distribution indicates the differing reaction pathways for SOA in fine and coarse modes.

We further explore the relationship between fine- and coarse-mode OOC and gaseous precursors, more details of the gaseous precursors are provided in the supporting information (Table S1). We observed a high correlation between fine-mode OOC and polar carbonyl compounds, such as glyoxal, methylglyoxal, acetone, and MVK+MACR (Table 1). Carbonyl compounds are first- and/or second-generation gas-phase oxidation products of both anthropogenic (e.g., aromatics, acetylene) and biogenic (e.g., isoprene) sources (Ervens et al., 2011), this also suggests a complex source profile for fine mode SOA. Additionally, carbonyl compounds have strong water solubility and can be absorbed into clouds and fog to react with $\cdot\text{OH}$ to form oligomers, which promote the formation of SOA (Wang et al., 2022). However, unlike the fine mode, we found that coarse-mode OOC is uniquely correlated with nonpolar aromatic hydrocarbons (e.g., toluene, C8 aromatic, C9 aromatic, styrene) and biogenic VOCs (e.g., monoterpenes, isoprene) (Table 1). This revealed different gaseous precursors for fine- and coarse-mode SOA, and reflected the different SOA generation mechanisms that may exist.

Table 1. The correlation coefficients between OOC and typical VOCs in the campaign. * indicates a significance level of 95% ($p < 0.05$).

	Monoterpenes	Isoprene	MVK+MACR	Toluene	C8 aromatic	C9 aromatic	Styrene	Glyoxal	Methylglyoxal	Acetone
Fine mode OOC	0.20	0.47	0.70*	0.38	0.39	0.36	0.46	0.70*	0.73*	0.62*
Coarse mode OOC	-0.75*	-0.56	-0.34	-0.60*	-0.65*	-0.66*	-0.74*	-0.39	-0.39	-0.52

3.3 Possible formation mechanisms for fine mode SOA

The previous results reveal a distinct origin for fine and coarse mode OOC, suggesting different SOA generation mechanisms. Therefore, additional field measurements are necessary to further



191 understand the mechanisms and key factors affecting SOA formation.

192 Building on the findings from the previous section that fine-mode OOC are primarily derived from
193 carbonyl compounds, it is noteworthy that carbonyl compounds are highly reactive and exhibit
194 significant water solubility (Liu et al., 2022; Wang et al., 2022; Xu et al., 2022). These properties enable
195 them to contribute significantly to SOA formation through aqueous-phase reactions, particularly for
196 dicarbonyls such as glyoxal (Gly, CHOCHO) and methylglyoxal (Mgly, CH₃COCHO), which have been
197 identified as key SOA precursors (Liu et al., 2022; Tan et al., 2017). Previous studies have identified
198 characteristic fragment ions of glyoxal and methylglyoxal (e.g., C₂O₂⁺ and CH₂O₂⁺), which play a crucial
199 role in the formation of low-volatility SOA during cloud processing and are strongly correlated with
200 aqueous oxygenated organic aerosol (aq-OOA) (Duan et al., 2020; Sun et al., 2016). As shown in Figure
201 4a, these fragment ions are predominantly distributed in fine particles, indicating the significance of
202 aqueous-phase processing in the fine mode. Further evidence of aqueous-phase reactions is provided by
203 the behavior of MVK and MACR. While the direct aqueous-phase reaction of MVK and MACR with
204 ozone is less competitive compared to the faster OH-initiated reactions (Chen et al., 2008), aerosol liquid
205 water content (ALWC) serves as a key metric for characterizing aqueous-phase SOA formation due to
206 its positive correlation with these processes, especially under conditions of high relative humidity and
207 elevated NO_x levels (Kuang et al., 2020b; McNeill, 2015; Zhan et al., 2021). In this study, we observed
208 a strong positive correlation between fine-mode OOC and ALWC (Figure 4b), suggesting that fine-mode
209 SOA is predominantly generated through aqueous-phase processes.

210 However, in contrast to the coarse mode, in contrast to the coarse modes, the fine modes are not
211 abundant in ALWC (Figure S4). Despite this, we observed a significant relationship between OOC and
212 ALWC exclusively in the fine mode. To further investigate the behavior of carbonyl compounds under



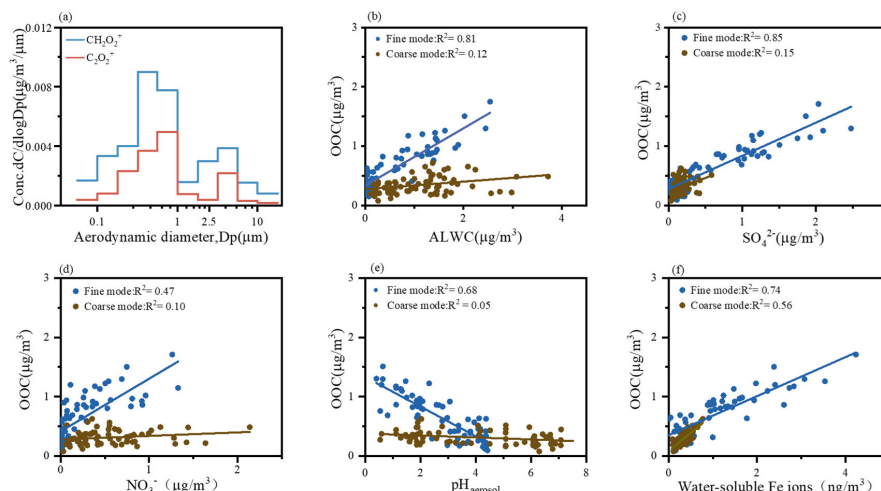
213 the unique conditions of the fine mode, we analyzed the correlations of fine- and coarse-mode OOC with
214 key factors, revealing notable differences between the two modes. First, the fine mode is characterized
215 by higher concentrations of inorganic ions, such as sulfate and nitrate, which may play a critical role in
216 SOA formation. Specifically, sulfate demonstrated a stronger positive influence on fine-mode OOC
217 formation compared to nitrate, as evidenced by their respective correlation coefficients ($R^2 = 0.85$ for
218 sulfate, Figure 4c; $R^2 = 0.47$ for nitrate, Figure 4d). This discrepancy may arise from the fact that sulfate
219 (SO_4^{2-}) is primarily produced through aqueous-phase reactions, whereas nitrate (NO_3^-) is predominantly
220 generated via gas-phase reactions (Zhan et al., 2021). Additionally, the fine mode exhibits acidic
221 conditions ($\text{pH}_{\text{aerosol}} = 0.4\text{--}4.3$), and we observed distinct correlations between fine-mode OOC and
222 $\text{pH}_{\text{aerosol}}$ (Figure 4e). This suggests that the lower pH in the fine mode favors the formation of fine-mode
223 OOC.

224 A few studies have emphasized the significant role of metal ions in SOA formation, particularly
225 under low pH conditions. To further investigate this, we examined the correlation between water-soluble
226 metal ions and fine-mode OOC (Table S5). Our analysis revealed that fine-mode OOC exhibits a strong
227 correlation with water-soluble Fe ions ($r = 0.82$, $p < 0.05$), and a positive relationship was observed
228 between the concentration of iron ions and fine-mode OOC (Figure 5f). Additionally, water-soluble iron
229 ions were found to be highly concentrated in the fine mode (Figure S4), with their concentration (18.87
230 ng/m^3) significantly exceeding that of other metal ions. Recent studies have highlighted the role of water-
231 soluble Fe ions in Fenton chemistry, where they cycle between Fe^{2+} and Fe^{3+} . This process, particularly
232 through Fenton reactions involving peroxides, may substantially enhance SOA formation by supplying
233 particle-phase oxidants (Qin et al., 2022; Ye et al., 2021). Specifically, Fenton reactions within aqueous
234 particles can generate hydroxyl radicals ($\text{OH}\cdot$), which oxidize organic compounds such as carbonyls,



235 especially under lower pH conditions (Kuang et al., 2020a).

236 Therefore, in this study, we propose that aqueous-phase reactions play a dominant role in the formation
237 of fine-mode SOA. The lower pH and elevated concentrations of water-soluble Fe ions in the fine mode
238 create favorable conditions for SOA formation from carbonyl compounds, primarily through Fenton
239 reactions.



240

241 **Figure 4.** Average size distributions of CH_2O_2^+ and C_2O_2^+ (a), and relationship between OOC and
242 ALWC (b), SO_4^{2-} (c), NO_3^- (d), $\text{pH}_{\text{aerosol}}$ (e), water-soluble iron ions(f)

243 3.4 Possible formation mechanisms for coarse mode SOA

244 Most studies have focused on the heterogeneous uptake of inorganic trace gases on dust particles, and
245 few studies have attempted to investigate the uptake of VOCs on mineral dust particles. To date, the
246 impact of authentic dust particles on SOA growth has been poorly studied, the mechanistic role of the
247 mineral dust in SOA growth is uncertain under typical polluted urban environments(Yu et al., 2016; Yu
248 and Jang, 2019).

249 A distinct phenomenon observed in our experiments is that biogenic-OOC are predominantly
250 distributed in the coarse mode, which may be attributed to unique SOA formation pathways in this mode.



251 Biogenic-OOC is primarily generated through the oxidation of biogenic volatile organic compounds
252 (BVOCs) by atmospheric oxidants such as hydroxyl radicals (OH), ozone (O₃), and nitrate radicals (NO₃)
253 (Gagan et al., 2023). BVOCs emitted by terrestrial vegetation, including isoprene and monoterpenes,
254 significantly contribute to the total SOA budget. As shown in Table 1, coarse-mode OOC exhibits a strong
255 correlation with monoterpenes ($r = -0.75$, $p < 0.05$) but a weaker correlation with isoprene ($r = -0.56$, p
256 < 0.05), suggesting that monoterpenes play a more prominent role in biogenic-OOC formation.

257 Regarding the mechanisms of SOA generation from monoterpenes and isoprene, isoprene primarily
258 reacts with OH radicals to form SOA, whereas monoterpenes, in addition to reacting with OH radicals,
259 also undergo significant SOA formation through reactions with O₃ (McFiggans et al., 2019; Xu et al.,
260 2015). Previous studies have demonstrated that monoterpene-derived SOA is more oxidized in the
261 presence of nitrate-containing seed aerosols compared to ammonium sulfate seed aerosols (Huang et al.,
262 2016; Watne et al., 2017). The higher nitrate concentrations in the coarse mode further favor the O₃
263 oxidation pathway for monoterpenes. Our sampling site, located in the Pearl River Delta (PRD) region,
264 is one of the most rapidly urbanized areas with high anthropogenic emissions (Ma et al., 2024). The
265 sampling period coincided with elevated O₃ pollution levels. Coarse-mode particles, characterized by
266 higher pH compared to fine-mode particles, create conditions conducive to photosensitive reactions and
267 O₃ oxidation pathways (Yu and Jang, 2019). Further analysis reveals a strong correlation between
268 coarse-mode OOC and O₃ (Figure 5a). Additionally, Figure 5b demonstrates that coarse-mode OOC
269 concentrations are significantly higher during high-O₃ periods compared to low-O₃ periods, with a
270 distinct peak observed during high-O₃ episodes. Notably, no significant increase in the concentrations of
271 other inorganic ions was observed during these high-O₃ periods (Figure S6). These findings collectively
272 underscore the critical role of O₃ in the formation of coarse-mode SOA.



273 However, the reaction pathways involved in coarse-mode secondary organic aerosol (SOA)
274 formation remain poorly understood. The ^{14}C isotope analysis results indicate that fossil fuel-derived
275 oxygenated organic compounds (OOC) are the primary source of coarse-mode OOC. Additionally,
276 coarse-mode OOC exhibits a stronger correlation with aromatic volatile organic compounds (VOCs),
277 particularly styrene (Table 1). However, since nonpolar aromatic hydrocarbons do not directly react with
278 O_3 to form SOA, further investigation is needed to elucidate the role of O_3 in coarse-mode SOA formation.
279 Recent studies have highlighted the rapid gas-phase autooxidation of endocyclic alkenes initiated by
280 ozonolysis, which yields highly oxygenated organic molecules (HOMs), particularly from monoterpenes
281 and aromatic compounds (Rissanen, 2021). Chemistry transport models have demonstrated that
282 ozonolysis of monoterpenes accounts for 79% of HOMs production (Shi et al., 2021). Additionally,
283 photochemical oxidation of substituted aromatic compounds has been shown to form HOMs through
284 rapid intramolecular autooxidation reactions, a process analogous to the oxidation of monoterpenes. O_3
285 can facilitate these reactions during the photo-oxidation of aromatics (Molteni et al., 2018; Suh et al.,
286 2003; Wang et al., 2020a), which partially explains the stronger correlation between O_3 and coarse-mode
287 OOC. This conclusion is further supported by the higher oxidation state (O/C ratio) observed in the coarse
288 mode compared to the fine mode (Figure 5c).

289 Moreover, recent studies have identified carboxylic acids as products of these reactions (Zhang et
290 al., 2017a). The slope of coarse-mode OOC in the Van Krevelen (VK) plot is close to -0.5 (Figure 5d),
291 indicating the large formation of carboxylic acids with fragmentation through the replacement of
292 hydrogen atoms. The coarse mode is characterized by higher ALWC, higher pH, and favorable
293 partitioning of reaction products into the particulate phase. Based on these findings, we propose that gas-
294 phase autooxidation plays a significant role in the formation of coarse-mode SOA.

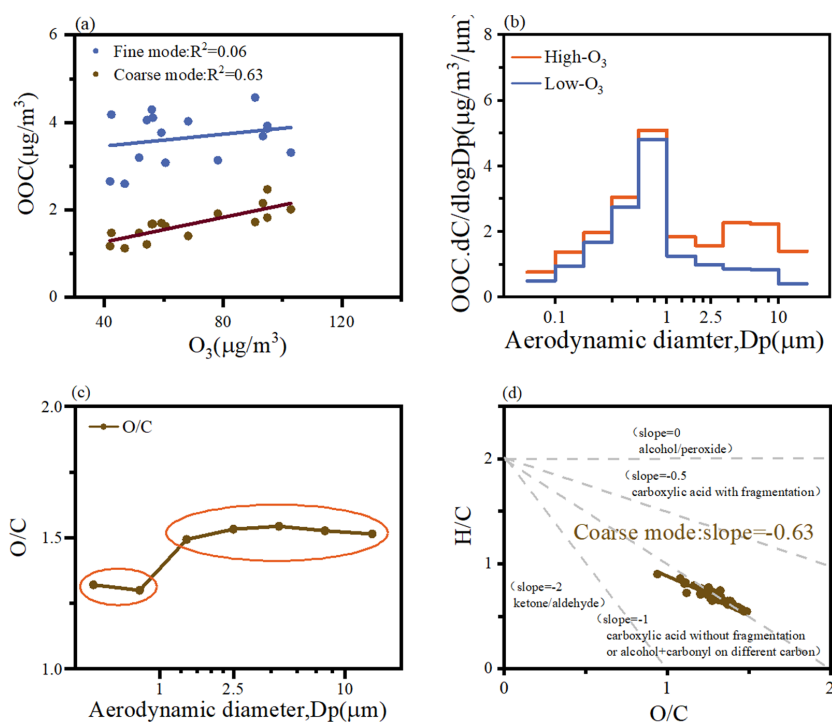


Figure 5. Relationship between OOC and O₃ (a), average size distributions of OOC (b), and organic

O/C(c), Van Krevelen diagram of H / C vs. O / C(d).

4 Summary and implications

This study collected 16 sets of size-segregated aerosol samples (0.056–18 μm) in Shenzhen, a coastal city in the Pearl River Delta, from October 2022 to January 2023. The water-soluble components, including typical inorganic ions, water-soluble organic compounds, and water-soluble metal ions, were analyzed, and water-soluble organic matter (WSOM) emerged as the most abundant water-soluble component in both modes, accounting for 55.9% and 40.9% of the total water-soluble mass in fine and coarse particles, respectively. This highlights the critical role of WSOM in both size fractions.

Our findings indicate that WSOM in both fine and coarse modes exhibits secondary production. To



306 quantify secondary organic aerosol (SOA), which is represented by oxygenated organic carbon (OOC),
307 we applied Positive Matrix Factorization (PMF) modeling and utilized radiocarbon isotopes to
308 distinguish between fossil fuel-derived and biogenic organic carbon (OOC). Radiocarbon (^{14}C) isotope
309 analysis reveals that fossil sources dominate SOA in both fine (95.8%) and coarse (80.4%) modes, while
310 the small amount of biogenic SOA mostly existed in the coarse mode (74.1%), we emphasize the
311 significant contribution of anthropogenic volatile organic compounds (VOCs) to SOA formation in
312 coastal atmospheres, where high relative humidity and enhanced atmospheric oxidation capacity also
313 play pivotal roles in SOA generation across both fine and coarse modes. Furthermore, we investigated
314 potential precursor sources for fine- and coarse-mode OOC, fine-mode oxygenated organic carbon (OOC)
315 correlates strongly with polar carbonyl compounds (e.g., glyoxal, methylglyoxal, acetone, and
316 MVK+MACR), while coarse-mode OOC exhibits better correlations with nonpolar aromatic
317 hydrocarbons (e.g., toluene, C8 aromatic, C9 aromatic, styrene) and biogenic VOCs (e.g., monoterpenes,
318 isoprene), indicating that the sources of fine- and coarse-mode OOC are different, indicating that the
319 sources of fine- and coarse-mode OOC are different, indicating distinct precursor sources for SOA in
320 different size modes.

321 Multivariate analyses incorporating inorganic ions, pH, water-soluble Fe ions, aerosol liquid water
322 content, and O_3 revealed divergent size-dependent mechanisms, emphasizing the significant role of
323 aqueous-phase reactions in fine-mode OOC formation, particularly the key contribution of water-soluble
324 iron ions ($r^2 = 0.74$), while coarse-mode OOC exhibited a notable correlation with O_3 ($r^2 = 0.63$).
325 Combining the information on VOCs precursors and key components, our study elucidates that aqueous-
326 phase reactions play a key role in fine-mode OOC, especially the Fenton reaction, while gas-phase
327 autoxidation plays an important role in the coarse-mode OOC generation. By examining OOC formation



328 across a wide range of particle sizes, this study provides novel insights into SOA formation mechanisms
329 and enhances our understanding of the formation pathways of SOA in both fine and coarse mode.
330 However, the specific mechanisms governing SOA generation in different particle size ranges remain
331 poorly understood. We strongly recommend further laboratory experiments to explore these mechanisms
332 in greater depth. Notably, our study underscores the significant role of anthropogenic VOCs in SOA
333 formation in coastal environments, where high relative humidity and atmospheric oxidation capacity are
334 critical drivers. Similar conditions are prevalent in marginal seas and estuaries near urban areas,
335 warranting further in-depth studies in these representative regions.
336



337 **Data availability.** Datasets are available by contacting the corresponding author, Meng-Xue Tang

338 (tangmx@pku.edu.cn)

339 **Supplement.** The supplement material related to this article is available online at:

340 **Author contributions.** WJ, TM and HX conceptualized the study. WJ, LS, and TJ executed the

341 experiments. WJ and TM carried out the statistical analysis. WJ prepared the first draft of the manuscript,

342 which was commented on and revised by TM and HX. All authors reviewed and approved the final

343 version for publication.

344 **Competing interests.** The authors declare that they have no conflict of interest.

345 **Financial support.** This work was supported by the National Key Research and Development Program

346 of China (2022YFC3701000, Task2) and the National Natural Science Foundation of China (42407145).

347



348 **Reference**

- 349 Adebisi, A., Kok, J. F., Murray, B. J., Ryder, C. L., Stuut, J.-B. W., Kahn, R. A., Knippertz, P., Formenti,
350 P., Mahowald, N. M., Pérez García-Pando, C., Klose, M., Ansmann, A., Samset, B. H., Ito, A.,
351 Balkanski, Y., Di Biagio, C., Romanias, M. N., Huang, Y., and Meng, J.: A review of coarse mineral
352 dust in the Earth system, *Aeolian Res.*, 60, 100849, <https://doi.org/10.1016/j.aeolia.2022.100849>,
353 2023.
- 354 Chen, Z. M., Wang, H. L., Zhu, L. H., Wang, C. X., Jie, C. Y., and Hua, W.: Aqueous-phase ozonolysis
355 of methacrolein and methyl vinyl ketone: a potentially important source of atmospheric aqueous
356 oxidants, *Atmos Chem Phys*, 8, 2255–2265, <https://doi.org/10.5194/acp-8-2255-2008>, 2008.
- 357 Dominutti, P. A., Chevassus, E., Baray, J.-L., Jaffrezo, J.-L., Borbon, A., Colomb, A., Deguillaume, L.,
358 El Gdachi, S., Houdier, S., Leriche, M., Metzger, J.-M., Rocco, M., Tulet, P., Sellegri, K., and Freney,
359 E.: Evaluation of the Sources, Precursors, and Processing of Aerosols at a High-Altitude Tropical
360 Site, *ACS Earth Space Chem.*, 6, 2412–2431, <https://doi.org/10.1021/acsearthspacechem.2c00149>,
361 2022.
- 362 Duan, J., Huang, R.J., Li, Y., Chen, Q., Zheng, Y., Chen, Y., Lin, C., Ni, H., Wang, M., Ovadnevaite, J.,
363 Ceburnis, D., Chen, C., Worsnop, D. R., Hoffmann, T., O'Dowd, C., and Cao, J.: Summertime and
364 wintertime atmospheric processes of secondary aerosol in Beijing, *Atmospheric Chem. Phys.*, 20,
365 3793–3807, <https://doi.org/10.5194/acp-20-3793-2020>, 2020.
- 366 Ervens, B., Turpin, B. J., and Weber, R. J.: Secondary organic aerosol formation in cloud droplets and
367 aqueous particles (aqSOA): a review of laboratory, field and model studies, *Atmospheric Chem. Phys.*,
368 11, 11069–11102, <https://doi.org/10.5194/acp-11-11069-2011>, 2011.
- 369 Gagan, S., Sarang, K., Rudzinski, K. J., Liu, R., Szmigielski, R., and Zhang, Y.: Synthetic strategies for
370 oxidation products from biogenic volatile organic compounds in the atmosphere: A review, *Atmos.*



- 371 Environ., 312, 120017, <https://doi.org/10.1016/j.atmosenv.2023.120017>, 2023.
- 372 George, C., Ammann, M., D'Anna, B., Donaldson, D. J., and Nizkorodov, S. A.: Heterogeneous
373 Photochemistry in the Atmosphere, *Chem. Rev.*, 115, 4218–4258, <https://doi.org/10.1021/cr500648z>,
374 2015.
- 375 Gu, Y., Huang, R.-J., Duan, J., Xu, W., Lin, C., Zhong, H., Wang, Y., Ni, H., Liu, Q., Xu, R., Wang, L.,
376 and Li, Y. J.: Multiple pathways for the formation of secondary organic aerosol in the North China
377 Plain in summer, *Atmospheric Chem. Phys.*, 23, 5419–5433, [https://doi.org/10.5194/acp-23-5419-](https://doi.org/10.5194/acp-23-5419-2023)
378 2023, 2023.
- 379 Hallquist, M., Wenger, J. C., Baltensperger, U., Rudich, Y., Simpson, D., Claeys, M., Dommen, J.,
380 Donahue, N. M., George, C., Goldstein, A. H., Hamilton, J. F., Herrmann, H., Hoffmann, T., Iinuma,
381 Y., Jang, M., Jenkin, M. E., Jimenez, J. L., Kiendler-Scharr, A., Maenhaut, W., McFiggans, G.,
382 Mentel, T. F., Monod, A., Prévôt, A. S. H., Seinfeld, J. H., Surratt, J. D., Szmigielski, R., and Wildt,
383 J.: The formation, properties and impact of secondary organic aerosol: current and emerging issues,
384 *Atmospheric Chem. Phys.*, 9, 5155–5236, <https://doi.org/10.5194/acp-9-5155-2009>, 2009.
- 385 He, D.Y., Huang, X.F., Wei, J., Wei, F.H., Zhu, B., Cao, L.M., and He, L.Y.: Soil dust as a potential
386 bridge from biogenic volatile organic compounds to secondary organic aerosol in a rural environment,
387 *Environ. Pollut.*, 298, 118840, <https://doi.org/10.1016/j.envpol.2022.118840>, 2022b.
- 388 Huang, D. D., Zhang, X., Dalleska, N. F., Lignell, H., Coggon, M. M., Chan, C., Flagan, R. C., Seinfeld,
389 J. H., and Chan, C. K.: A note on the effects of inorganic seed aerosol on the oxidation state of
390 secondary organic aerosol— α -Pinene ozonolysis, *J. Geophys. Res. Atmospheres*, 121,
391 <https://doi.org/10.1002/2016JD025999>, 2016.
- 392 Huang, X.F., Dai, J., Zhu, Q., Yu, K., and Du, K.: Abundant Biogenic Oxygenated Organic Aerosol in



393 Atmospheric Coarse Particles: Plausible Sources and Atmospheric Implications, Environ. Sci.
394 Technol., 54, 1425–1430, <https://doi.org/10.1021/acs.est.9b06311>, 2020.

395 Jimenez, J. L., Canagaratna, M. R., Donahue, N. M., Prevot, A. S. H., Zhang, Q., Kroll, J. H., DeCarlo,
396 P. F., Allan, J. D., Coe, H., Ng, N. L., Aiken, A. C., Docherty, K. S., Ulbrich, I. M., Grieshop, A. P.,
397 Robinson, A. L., Duplissy, J., Smith, J. D., Wilson, K. R., Lanz, V. A., Hueglin, C., Sun, Y. L., Tian,
398 J., Laaksonen, A., Raatikainen, T., Rautiainen, J., Vaattovaara, P., Ehn, M., Kulmala, M., Tomlinson,
399 J. M., Collins, D. R., Cubison, M. J., E., Dunlea, J., Huffman, J. A., Onasch, T. B., Alfarra, M. R.,
400 Williams, P. I., Bower, K., Kondo, Y., Schneider, J., Drewnick, F., Borrmann, S., Weimer, S.,
401 Demerjian, K., Salcedo, D., Cottrell, L., Griffin, R., Takami, A., Miyoshi, T., Hatakeyama, S.,
402 Shimono, A., Sun, J. Y., Zhang, Y. M., Dzepina, K., Kimmel, J. R., Sueper, D., Jayne, J. T., Herndon,
403 S. C., Trimborn, A. M., Williams, L. R., Wood, E. C., Middlebrook, A. M., Kolb, C. E., Baltensperger,
404 U., and Worsnop, D. R.: Evolution of Organic Aerosols in the Atmosphere, Science, 326, 1525–1529,
405 <https://doi.org/10.1126/science.1180353>, 2009.

406 Kuang, X. M., Gonzalez, D. H., Scott, J. A., Vu, K., Hasson, A., Charbouillot, T., Hawkins, L., and
407 Paulson, S. E.: Cloud Water Chemistry Associated with Urban Aerosols: Rapid Hydroxyl Radical
408 Formation, Soluble Metals, Fe(II), Fe(III), and Quinones, ACS Earth Space Chem., 4, 67–76,
409 <https://doi.org/10.1021/acsearthspacechem.9b00243>, 2020a.

410 Kuang, Y., He, Y., Xu, W., Yuan, B., Zhang, G., Ma, Z., Wu, C., Wang, C., Wang, S., Zhang, S., Tao,
411 J., Ma, N., Su, H., Cheng, Y., Shao, M., and Sun, Y.: Photochemical Aqueous-Phase Reactions Induce
412 Rapid Daytime Formation of Oxygenated Organic Aerosol on the North China Plain, Environ. Sci.
413 Technol., 54, 3849–3860, <https://doi.org/10.1021/acs.est.9b06836>, 2020b.

414 Li, W. J. and Shao, L. Y.: Observation of nitrate coatings on atmospheric mineral dust particles, Atmos



- 415 Chem Phys, 9, 1863–1871, <https://doi.org/10.5194/acp-9-1863-2009>, 2009.
- 416 Li, Z.J., He, L.Y., Ma, H.N., Peng, X., Tang, M.X., Du, K., and Huang, X.-F.: Sources of atmospheric
417 oxygenated volatile organic compounds in different air masses in Shenzhen, China, Environ. Pollut.,
418 340, 122871, <https://doi.org/10.1016/j.envpol.2023.122871>, 2024a.
- 419 Liu, Q., Gao, Y., Huang, W., Ling, Z., Wang, Z., and Wang, X.: Carbonyl compounds in the atmosphere:
420 A review of abundance, source and their contributions to O₃ and SOA formation, Atmospheric Res.,
421 274, 106184, <https://doi.org/10.1016/j.atmosres.2022.106184>, 2022.
- 422 Ma, F., Wang, H., Ding, Y., Zhang, S., Wu, G., Li, Y., Gong, D., Ristovski, Z., He, C., and Wang, B.:
423 Amplified Secondary Organic Aerosol Formation Induced by Anthropogenic–Biogenic Interactions
424 in Forests Around Megacities, J. Geophys. Res. Atmospheres, 129, e2024JD041679,
425 <https://doi.org/10.1029/2024JD041679>, 2024.
- 426 McFiggans, G., Mentel, T. F., Wildt, J., Pullinen, I., Kang, S., Kleist, E., Schmitt, S., Springer, M.,
427 Tillmann, R., Wu, C., Zhao, D., Hallquist, M., Faxon, C., Le Breton, M., Hallquist, Å. M., Simpson,
428 D., Bergström, R., Jenkin, M. E., Ehn, M., Thornton, J. A., Alfarra, M. R., Bannan, T. J., Percival, C.
429 J., Priestley, M., Topping, D., and Kiendler-Scharr, A.: Secondary organic aerosol reduced by mixture
430 of atmospheric vapours, Nature, 565, 587–593, <https://doi.org/10.1038/s41586-018-0871-y>, 2019.
- 431 McNeill, V. F.: Aqueous Organic Chemistry in the Atmosphere: Sources and Chemical Processing of
432 Organic Aerosols, Environ. Sci. Technol., 49, 1237–1244, <https://doi.org/10.1021/es5043707>, 2015.
- 433 Mei, S., Xia, K., Liu, C., Chen, X., Yuan, R., Liu, H., Zhao, C., and Liu, S.: Aqueous-Phase Processing
434 Affects the Formation and Size Distribution of Aerosol Organic Functional Groups During Heavy
435 Pollution, J. Geophys. Res. Atmospheres, 130, e2024JD042029,
436 <https://doi.org/10.1029/2024JD042029>, 2025.



- 437 Molteni, U., Bianchi, F., Klein, F., El Haddad, I., Frege, C., Rossi, M. J., Dommen, J., and Baltensperger,
438 U.: Formation of highly oxygenated organic molecules from aromatic compounds, *Atmospheric*
439 *Chem. Phys.*, 18, 1909–1921, <https://doi.org/10.5194/acp-18-1909-2018>, 2018.
- 440 Pan, Y., Quan, J., Ma, P., Liao, Z., Jia, X., Dou, Y., Cheng, Z., Lei, L., Wang, Y., Zheng, M., Lü, D., and
441 Wang, Y.: Mineral dust scavenges anthropogenic aerosols in polluted environment, *Atmos. Environ.*,
442 309, 119938, <https://doi.org/10.1016/j.atmosenv.2023.119938>, 2023.
- 443 Peng, J., Hu, M., Shang, D., Wu, Z., Du, Z., Tan, T., Wang, Y., Zhang, F., and Zhang, R.: Explosive
444 Secondary Aerosol Formation during Severe Haze in the North China Plain, *Environ. Sci. Technol.*,
445 55, 2189–2207, <https://doi.org/10.1021/acs.est.0c07204>, 2021.
- 446 Qin, X., Chen, Z., Gong, Y., Dong, P., Cao, Z., Hu, J., and Xu, J.: Persistent Uptake of H₂ O₂ onto
447 Ambient PM_{2.5} via Dark-Fenton Chemistry, *Environ. Sci. Technol.*, 56, 9978–9987,
448 <https://doi.org/10.1021/acs.est.2c03630>, 2022.
- 449 Rissanen, M.: Anthropogenic Volatile Organic Compound (AVOC) Autoxidation as a Source of Highly
450 Oxygenated Organic Molecules (HOM), *J. Phys. Chem. A*, 125, 9027–9039,
451 <https://doi.org/10.1021/acs.jpca.1c06465>, 2021.
- 452 Shi, X., Huang, G., Yang, D., Zhang, Q., Zong, W., Cheng, J., Sui, X., Yuan, F., and Wang, W.:
453 Theoretical study of the formation and nucleation mechanism of highly oxygenated multi-functional
454 organic compounds produced by α -pinene, *Sci. Total Environ.*, 780, 146422,
455 <https://doi.org/10.1016/j.scitotenv.2021.146422>, 2021.
- 456 Suh, I., Zhang, R., Molina, L. T., and Molina, M. J.: Oxidation Mechanism of Aromatic Peroxy and
457 Bicyclic Radicals from OH-Toluene Reactions, *J. Am. Chem. Soc.*, 125, 12655–12665,
458 <https://doi.org/10.1021/ja0350280>, 2003.



- 459 Sun, Y., Du, W., Fu, P., Wang, Q., Li, J., Ge, X., Zhang, Q., Zhu, C., Ren, L., Xu, W., Zhao, J., Han, T.,
460 Worsnop, D. R., and Wang, Z.: Primary and secondary aerosols in Beijing in winter: sources,
461 variations and processes, *Atmospheric Chem. Phys.*, 16, 8309–8329, [https://doi.org/10.5194/acp-16-](https://doi.org/10.5194/acp-16-8309-2016)
462 8309-2016, 2016.
- 463 Tan, H., Cai, M., Fan, Q., Liu, L., Li, F., Chan, P. W., Deng, X., and Wu, D.: An analysis of aerosol
464 liquid water content and related impact factors in Pearl River Delta, *Sci. Total Environ.*, 579, 1822–
465 1830, <https://doi.org/10.1016/j.scitotenv.2016.11.167>, 2017.
- 466 Wang, J., Chen, S., Qiu, X., Niu, W., Li, O., Zhu, C., Zhang, X., Yang, X., and Zhang, G.: Pollution
467 Characteristics of Atmospheric Carbonyl Compounds in a Large City of Northern China, *J. Chem.*,
468 2022, 1–13, <https://doi.org/10.1155/2022/3292598>, 2022.
- 469 Wang, S., Newland, M. J., Deng, W., Rickard, A. R., Hamilton, J. F., Muñoz, A., Ródenas, M., Vázquez,
470 M. M., Wang, L., and Wang, X.: Aromatic Photo-oxidation, A New Source of Atmospheric Acidity,
471 *Env. Sci Technol.*, 2020a.
- 472 Wang, T., Liu, Y., Deng, Y., Cheng, H., Yang, Y., Feng, Y., Zhang, L., Fu, H., and Chen, J.:
473 Photochemical Oxidation of Water-Soluble Organic Carbon (WSOC) on Mineral Dust and Enhanced
474 Organic Ammonium Formation, *Environ. Sci. Technol.*, 54, 15631–15642,
475 <https://doi.org/10.1021/acs.est.0c04616>, 2020b.
- 476 Watne, Å. K., Westerlund, J., Hallquist, Å. M., Brune, W. H., and Hallquist, M.: Ozone and OH-induced
477 oxidation of monoterpenes: Changes in the thermal properties of secondary organic aerosol (SOA),
478 *J. Aerosol Sci.*, 114, 31–41, <https://doi.org/10.1016/j.jaerosci.2017.08.011>, 2017.
- 479 Wu, X., Kong, Q., Lan, Y., Sng, J., and Yu, L. E.: Refined Sea Salt Markers for Coastal Cities Facilitating
480 Quantification of Aerosol Aging and PM_{2.5} Apportionment, *Environ. Sci. Technol.*,



- 481 <https://doi.org/10.1021/acs.est.3c10142>, 2024.
- 482 Xu, B., Zhang, G., Gustafsson, Ö., Kawamura, K., Li, J., Andersson, A., Bikkina, S., Kunwar, B., Pokhrel,
483 A., Zhong, G., Zhao, S., Li, J., Huang, C., Cheng, Z., Zhu, S., Peng, P., and Sheng, G.: Large
484 contribution of fossil-derived components to aqueous secondary organic aerosols in China, *Nat.*
485 *Commun.*, 13, 5115, <https://doi.org/10.1038/s41467-022-32863-3>, 2022.
- 486 Xu, L., Guo, H., Boyd, C. M., Klein, M., Bougiatioti, A., Cerully, K. M., Hite, J. R., Isaacman-VanWertz,
487 G., Kreisberg, N. M., Knote, C., Olson, K., Koss, A., Goldstein, A. H., Hering, S. V., De Gouw, J.,
488 Baumann, K., Lee, S.-H., Nenes, A., Weber, R. J., and Ng, N. L.: Effects of anthropogenic emissions
489 on aerosol formation from isoprene and monoterpenes in the southeastern United States, *Proc. Natl.*
490 *Acad. Sci.*, 112, 37–42, <https://doi.org/10.1073/pnas.1417609112>, 2015.
- 491 Xu, M., Hu, B., Zhao, S., Yan, G., Wen, T., and Zhao, X.: Size-resolved water-soluble organic carbon
492 and its significant contribution to aerosol liquid water, *Sci. Total Environ.*, 927, 172396,
493 <https://doi.org/10.1016/j.scitotenv.2024.172396>, 2024.
- 494 Xu, W., Han, T., Du, W., Wang, Q., Chen, C., Zhao, J., Zhang, Y., Li, J., Fu, P., Wang, Z., Worsnop, D.
495 R., and Sun, Y.: Effects of Aqueous-Phase and Photochemical Processing on Secondary Organic
496 Aerosol Formation and Evolution in Beijing, China, *Environ. Sci. Technol.*, 51, 762–770,
497 <https://doi.org/10.1021/acs.est.6b04498>, 2017.
- 498 Yang, W., Ma, J., Yang, H., Li, F., and Han, C.: Photoenhanced sulfate formation by the heterogeneous
499 uptake of SO₂ on non-photoactive mineral dust, *Atmospheric Chem. Phys.*, 24, 6757–6768,
500 <https://doi.org/10.5194/acp-24-6757-2024>, 2024.
- 501 Yao, D., Guo, H., Lyu, X., Lu, H., and Huo, Y.: Secondary organic aerosol formation at an urban
502 background site on the coastline of South China: Precursors and aging processes, *Environ. Pollut.*,



- 503 309, 119778, <https://doi.org/10.1016/j.envpol.2022.119778>, 2022.
- 504 Ye, C., Chen, H., Hoffmann, E. H., Mettke, P., Tilgner, A., He, L., Mutzel, A., Brüggemann, M., Poulain,
505 L., Schaefer, T., Heinold, B., Ma, Z., Liu, P., Xue, C., Zhao, X., Zhang, C., Zhang, F., Sun, H., Li,
506 Q., Wang, L., Yang, X., Wang, J., Liu, C., Xing, C., Mu, Y., Chen, J., and Herrmann, H.: Particle-
507 Phase Photoreactions of HULIS and TMs Establish a Strong Source of H₂O₂ and Particulate Sulfate
508 in the Winter North China Plain, Environ. Sci. Technol., 55, 7818–7830,
509 <https://doi.org/10.1021/acs.est.1c00561>, 2021.
- 510 Yu, G.H., Park, S., and Lee, K.H.: Source contributions and potential source regions of size-resolved
511 water-soluble organic carbon measured at an urban site over one year, Environ. Sci. Process. Impacts,
512 18, 1343–1358, <https://doi.org/10.1039/C6EM00416D>, 2016.
- 513 Yu, Z. and Jang, M.: Atmospheric Processes of Aromatic Hydrocarbons in the Presence of Mineral Dust
514 Particles in an Urban Environment, ACS Earth Space Chem., 2019.
- 515 Zhan, B., Zhong, H., Chen, H., Chen, Y., Li, X., Wang, L., Wang, X., Mu, Y., Huang, R.-J., George, C.,
516 and Chen, J.: The roles of aqueous-phase chemistry and photochemical oxidation in oxygenated
517 organic aerosols formation, Atmos. Environ., 266, 118738,
518 <https://doi.org/10.1016/j.atmosenv.2021.118738>, 2021.
- 519 Zhang, X., Lambe, A. T., Upshur, M. A., Brooks, W. A., Gray Bé, A., Thomson, R. J., Geiger, F. M.,
520 Surratt, J. D., Zhang, Z., Gold, A., Graf, S., Cubison, M. J., Groessl, M., Jayne, J. T., Worsnop, D.
521 R., and Canagaratna, M. R.: Highly Oxygenated Multifunctional Compounds in α -Pinene Secondary
522 Organic Aerosol, Environ. Sci. Technol., 51, 5932–5940, <https://doi.org/10.1021/acs.est.6b06588>,
523 2017a.
- 524 Zhang, Y., Cai, J., Wang, S., He, K., and Zheng, M.: Review of receptor-based source apportionment



525 research of fine particulate matter and its challenges in China, Sci. Total Environ., 586, 917–929,

526 <https://doi.org/10.1016/j.scitotenv.2017.02.071>, 2017b.

527